Calculated fission yields of neutron-deficient mercury isotopes

Peter Möller, Jørgen Randrup, and Arnold J. Sierk

Phys. Rev. C **85**, 024306 — Published 10 February 2012

DOI: 10.1103/PhysRevC.85.024306

Calculated fission yields of neutron-deficient mercury isotopes

Peter Möller[1],* Jørgen Randrup[2], and Arnold J. Sierk[1]
[1] *Theoretical Division, Los Alamos National Laboratory, Los Alamos, New Mexico 87545, USA*
[2] *Nuclear Science Division, Lawrence Berkeley National Laboratory, Berkeley, California 94720, USA*
(Dated: January 12, 2012)

The recent unexpected discovery of asymmetric fission of ^{180}Hg following the electron-capture decay of ^{180}Tl has led to intense interest in experimentally mapping the fission-yield properties over more extended regions of the nuclear chart and compound-system energies. We present here a first calculation of fission-fragment yields for neutron-deficient Hg isotopes, using the recently developed Brownian Metropolis shape motion treatment. The results for ^{180}Hg are in approximate agreement with the experimental data. For ^{174}Hg the symmetric yield increases strongly with decreasing energy, an unusual feature, which would be interesting to verify experimentally.
PACS numbers: 25.85.-w, 24.10.Lx,24.75.+

I. INTRODUCTION

After the seminal experimental studies by Schmidt and collaborators [1] on fission yields of neutron-deficient isotopes in the range $85 \leq Z \leq 92$, it was often assumed that fission yields in the heavy-element region were well mapped out and understood: asymmetric fission in most of the actinide region, onset of symmetric fission above $A \approx 258$ and below $A \approx 226$. However, in earlier, more limited studies, for lower proton numbers near $Z = 82$ and nucleon numbers near $A = 200$ hints of asymmetric fission had been reported at energies about 10 MeV above the barrier saddle energy [2, 3]. As is the case in many proposed models of heavy-element fission yields [4, 5], also here explanations in terms of fragment shells were proposed [6]. The recent discovery of asymmetric fission of ^{180}Hg, following electron capture (EC) on ^{180}Tl and associated theoretical study [7] showed that fission yields could not be simply connected to fragment shell properties. Arguments based on fragment shells had anticipated symmetric fission for this system, which would lead to two fragments with 50 neutrons each, namely two ^{90}Zr fission fragments. In contrast to fragment-shell arguments, it is necessary to take into account how the system evolves to the final state of separated nuclei, and not just base models on the energies of the possible final states [8]. Such a theory needs to involve the potential energy between the ground-state and the separated fragments, a principle already invoked by Bohr [9] immediately after the discovery of fission. To this day, this picture remains a pillar of fission theory and is invoked in all fundamental approaches, for example Refs. [10–14]. We have given further, more complete comments on other potential-energy and fission-yield calculations in Refs. [8, 15, 16].

The observed *asymmetric* fission of ^{180}Hg, while not anticipated, can be understood on the basis of the associated fission potential-energy surface calculated as a function of five shape degrees of freedom [7, 12]. This shape family includes all shapes within the three-quadratic surface parameterization that were expected to be relevant in the evolution of the system from the ground-state shape to shapes in the vicinity of scission, where the system divides into two distinct fragments. The specific features of the calculated potential-energy landscape for ^{180}Hg made it possible to offer a theoretical explanation, from static considerations alone, why an asymmetric yield was observed in this experiment [7]. But calculated potential-energy surfaces for other systems often have structures that do not allow similar unambiguous conclusions about fission-fragment mass asymmetry. In Ref. [7] no general method for obtaining fission-fragment mass distributions based on these surfaces was introduced.

To overcome the limitations of phenomenological and simple static-only approaches, we have recently developed a method based on a more microscopic foundation, namely Brownian shape motion on five-dimensional (5D) potential-energy surfaces. In benchmark studies it has been shown to describe fission-fragment yields along isotope chains where the yield properties rapidly change [8, 16, 17]. We apply this method in its simple Metropolis random-walk approximation [8], BSM(M), to the new region of interest in fission, namely neutron-deficient Hg isotopes and present calculated results for eight even-even isotopes, ^{174}Hg–^{188}Hg, for three compound-nucleus excitation energies: near-barrier energies ($B_{\rm f}$ + 2 MeV), 20 MeV, and 40 MeV. Because the BSM(M) yields are sensitive to the detailed structure of the 5D surfaces, it is useful to review some aspects of their structure as well as EC-delayed fission. We calculate the yield for eight isotopes but will refer extensively to ^{180}Hg for illustrative examples.

II. ELECTRON CAPTURE

When ^{180}Tl EC decays to daughter states in ^{180}Hg, energy levels from the ground state up to an energy $Q_{\rm EC}$ may be populated. These states subsequently decay by

* moller@lanl.gov

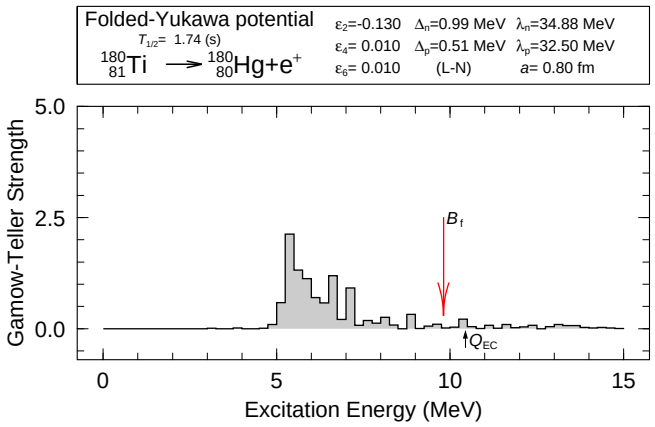

FIG. 1. (Color online) Calculated β-strength function for EC capture on $^{180}_{81}$Tl$_{99}$. The 1.74 s calculated half-life agrees well with the experimental 1.5 ± 0.2 s half-life [19]. Only states below $Q_{\rm EC}$ will be populated. The calculated barrier height of $^{180}_{80}$Hg$_{100}$ [14] is indicated by the arrow $B_{\rm f}$. Only states from a few MeV below $B_{\rm f}$ up to $Q_{\rm EC}$ will have a measurable fission branch. The important parameters [20] of the calculation and the underlying model are specified in the upper panel.

(1) γ de-excitation, (2) proton emission, (3) α emission, or (4) fission. The EC decay intensity to a level at energy $E_{\rm ex}$ in the daughter is proportional to a product of the square of the nuclear matrix element, or β-strength function, and a phase-space factor, which is roughly proportional to $(Q_{\rm EC} - E_{\rm ex})^5$ [18]. We show in Fig. 1 the calculated strength function for EC on ^{180}Tl. The calculation is based on a quasi-particle random-phase approximation [20–22]. The deformation used is the deformation of the daughter ground state. Branching ratios to different decay modes from the daughter ^{180}Hg can be calculated approximately. However, these calculations are complicated by the occurrence of shape coexistence in ^{180}Hg. Figure 2 (taken from Ref. [23] where further details of the calculation are given) shows a calculated potential-energy surface for shapes near the ground state of ^{180}Hg. Prolate shapes are along the horizontal axis, oblate shapes along the 60-degree axis, and axially asymmetric shapes in the interior of the plot. Two minima of near-equal energy exist, one near-oblate minimum at $\epsilon_2 = 0.125$ and $\gamma = 50^\circ$ and one prolate minimum at $\epsilon_2 = 0.225$ and $\gamma = 0^\circ$.

Here we do not focus on the branching between various decay modes in the daughter, but take advantage of the unique properties of electron-capture-delayed fission to learn about low-energy fission in this region of the nuclear chart. Due to the phase-space factor, only a very small fraction of the EC decays will lead to states above the fission barrier. At these high energies the positions of the nuclear levels, as calculated in any model, are not very accurate. Nevertheless, because of the fifth power in the phase-space factor, most of the fission decays leading to the observed yield distribution arise from fission following barrier penetration at energies one or two MeV below the saddle energy.

III. FIVE-DIMENSIONAL POTENTIAL-ENERGY SURFACES

The calculated macroscopic-microscopic 5D surfaces are significantly more complex than 2D macroscopic surfaces, which have previously been used to understand some aspects of nuclear fission [24, 25]. We have earlier observed that microscopic effects are so significant that an accurate description of them in 5D is necessary to model fission barriers and fission-fragment yields [8, 12, 14, 16].

To illustrate that some prominent structural features of these surfaces change significantly along the isotope sequence ^{174}Hg–^{188}Hg we show in Figs. 3–5 key features in the potential-energy surfaces for three representative nuclei, namely ^{174}Hg, ^{180}Hg, and ^{188}Hg. These features have been determined by use of the immersion technique applied to the full 5D surface, as described in Refs. [12, 14]. The downward-pointing triangles indicate all minima deeper than 0.2 MeV. Upward-pointing triangles are all optimal saddles between all such pairs of minima. Nuclear shapes at locations of special interest are also shown. The solid line labeled "Fission Barrier" has been calculated in a constrained β (multipole) parameterization up to $(Q_2/{\rm b})^{(1/2)} \approx 7$. This method

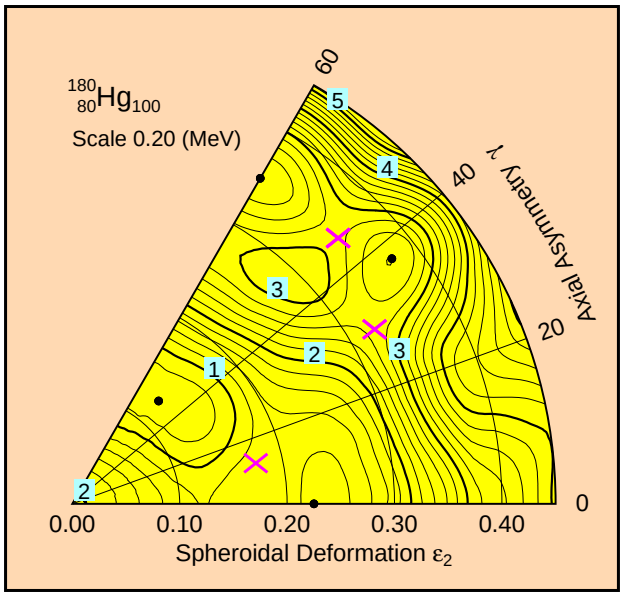

FIG. 2. (Color online) Calculated potential-energy surface of $^{180}_{80}$Hg$_{100}$. This nucleus exhibits quadruple shape coexistence. Minima are marked with solid dots. Optimal saddles between pairs of minima are marked with crosses. The ground state is situated at the lowest minimum, $\epsilon_2 = 0.125$ and $\gamma = 50^\circ$.

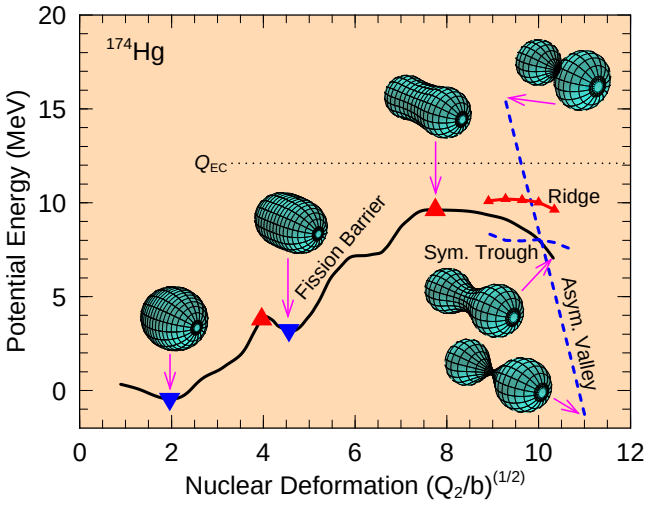

FIG. 3. (Color online) Minima, saddles, major valleys and ridges in the 5D potential-energy surface of ^{174}Hg (see text). At the last plotted point on the fission barrier, $(Q_2/\mathrm{b})^{(1/2)} \approx 10.5$, the asymmetry of the shape is $A_\mathrm{H}/A_\mathrm{L} = 104/70$.

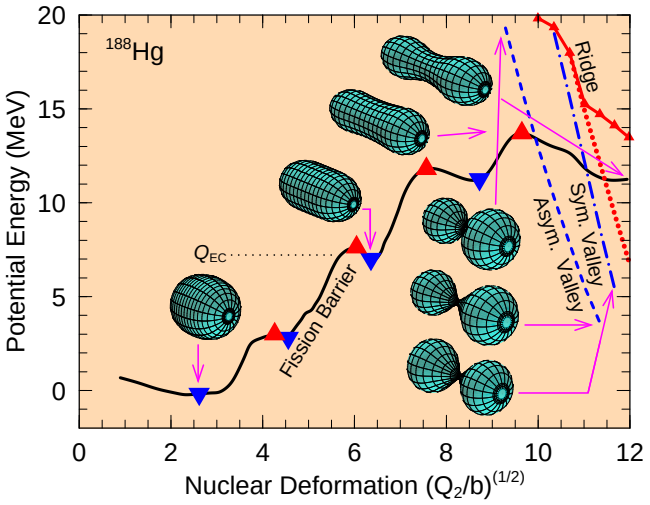

FIG. 5. (Color online) Minima, saddles, major valleys, and major ridges in the 5D potential-energy surface of ^{188}Hg. The ridge indicated by a solid line with triangles is the ridge between the fission barrier and both of the valleys. For low Q_2 it is also the ridge between the two valleys. For higher Q_2 there is a bifurcation and the ridge between the two valleys is given by the dotted line. At the last plotted point on the fission barrier, $(Q_2/\mathrm{b})^{(1/2)} = 12$, the asymmetry of the shape is $A_\mathrm{H}/A_\mathrm{L} = 111/77$.

can be quite deficient, in particular for large deformations beyond that value, see Ref. [14] for details. For example, slight changes in the definition of the elongation constraint result in radically different barriers and saddle-point heights. However, in this case, at small deformations, the curve overlaps perfectly with the saddles and minima found by correct methods in the full 5D calculations, so we use this curve to define, for illustrative purposes, a one-dimensional fission barrier for $(Q_2/\mathrm{b})^{(1/2)} \leq 7$. Next we connect this curve by spline

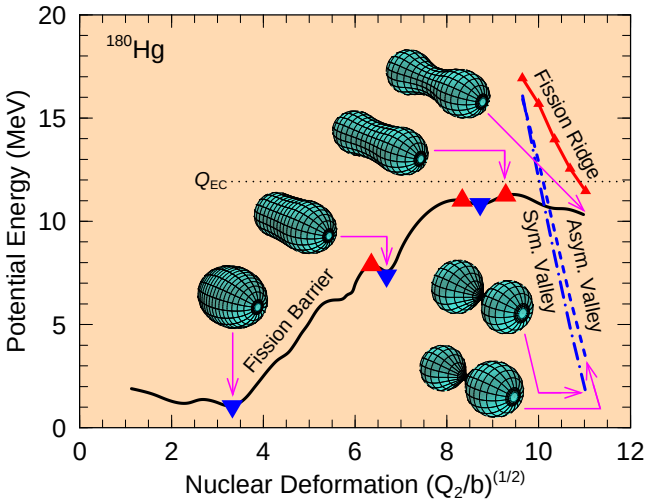

FIG. 4. (Color online) Minima, saddles, major valleys and ridges in the 5D potential-energy surface of ^{180}Hg (see text). At the last plotted point on the fission barrier, $(Q_2/\mathrm{b})^{(1/2)} \approx 11$, the asymmetry of the shape is $A_\mathrm{H}/A_\mathrm{L} = 108/72$.

interpolation to the subsequent two saddles and the intermediate minimum (one saddle only for ^{174}Hg) near $(Q_2/\mathrm{b})^{(1/2)} = 9$. Beyond the outer saddle the curve is defined by the bottom of the fission valley, identified as that valley along which nuclear shapes are most similar to the saddle-point shape.

For ^{174}Hg in Fig. 3, the potential-energy surface is relatively simple. The "fission barrier" path loses stability with respect to some of the four additional shape degrees of freedom just beyond $(Q_2/\mathrm{b})^{1/2} = 10$, because the ridge disappears here. At this and nearby elongations a symmetric trough exists in the potential surface. The fission valley is stabilized with respect to this trough by a low ridge indicated by a solid line with upward-pointing triangles. At larger deformation the minimum energy is an asymmetric valley with $A_\mathrm{H}/A_\mathrm{L} \approx 113/61$. Other valleys exist at higher energies but are not very prominent because they are only weakly stabilized by rather low ridges that are only about 0.5 MeV high. In EC-delayed fission following EC on ^{174}Tl a 2.5-MeV energy range above the barrier would be accessible.

For ^{180}Hg in Fig. 4 more prominent, higher ridges and and deeper valleys are present than for ^{174}Hg in Fig. 3. The deepest and most persistent valleys in the surface are an asymmetric (dashed) and a symmetric (dot-dashed) valley. These valleys are referred to as fusion valleys because they appear at large deformations and correspond to zero neck radius and specific mass divisions, or equivalently targets and projectiles. The valleys and ridges are

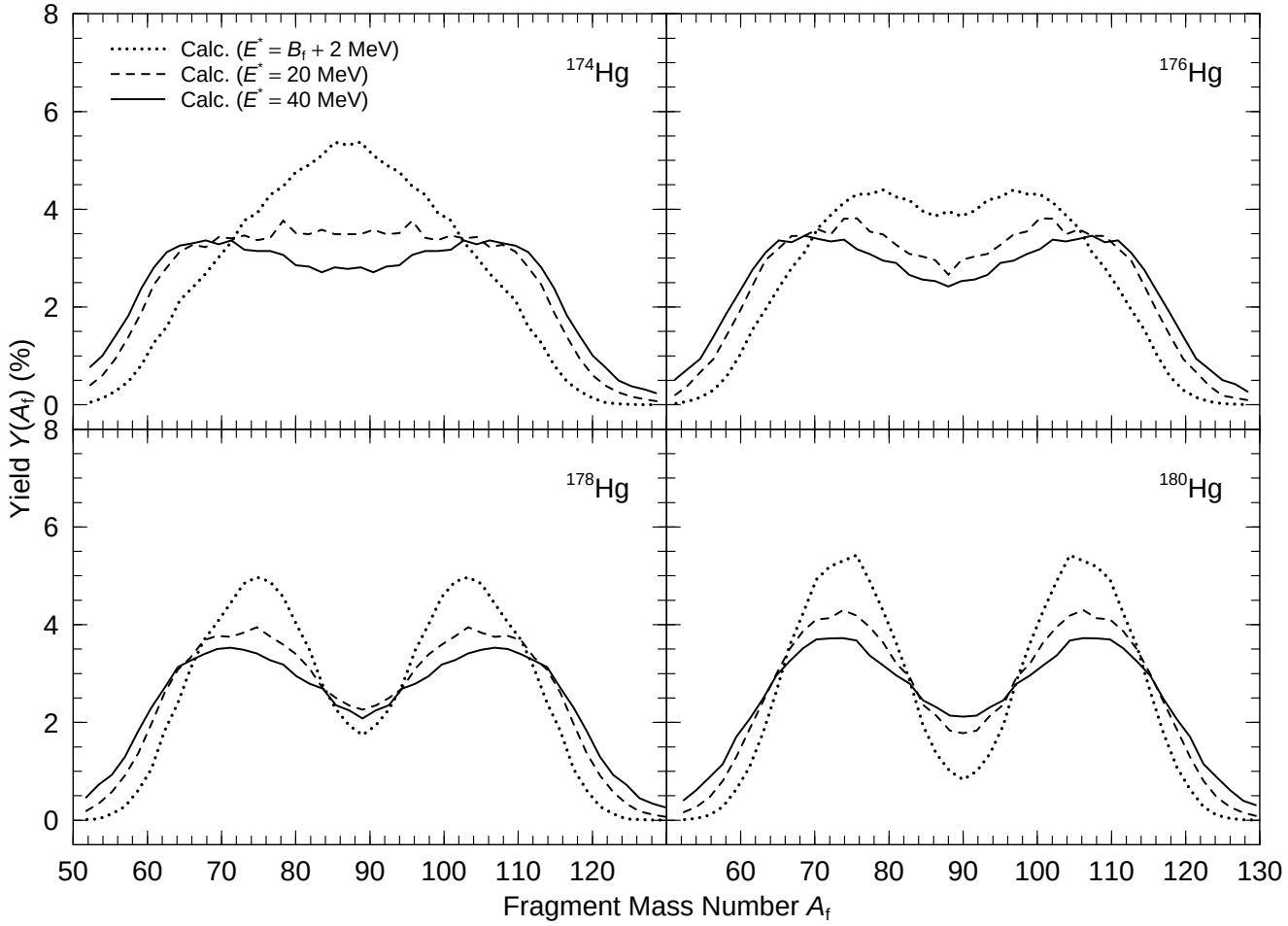

FIG. 6. Calculated yields for four Hg isotopes at three excitation energies. All yield curves are based on 50000 trajectories. For the lighter isotopes the yields become more symmetric with decreasing energy, an unusual behavior.

also more prominent than in the macroscopic 2D calculation shown in Fig. 11 in Ref. [24], for a nearby system. For ^{180}Hg in Fig. 4 the fission saddle and fission valley just beyond are separated from the fusion valleys by a ridge that initially, at the saddle, is more than five MeV high. The ridge rapidly decreases in height as the system elongates and at $(Q_2/\mathrm{b})^{(1/2)} \approx 11$ the fission valley ends. This is somewhat similar to the disappearance of the fission valley at $r \approx 2.3$ in the macroscopic potential-energy surface in Fig. 11 of Ref. [24]. In EC-delayed fission Q_{EC} is so low that only the fission-barrier valley is accessible for elongations less than $(Q_2/\mathrm{b})^{(1/2)} \approx 11$ because access to other valleys is blocked by high ridges. At this value of Q_2 a quite well-developed neck has formed and it is reasonable to expect that the nucleus at this point is close to dividing into two separate fragments with the mass division of this configuration, namely $A_{\mathrm{H}}/A_{\mathrm{L}} = 108/72$, defined as described in Ref. [12]. Further discussion is in Ref. [7].

Equally prominent features are present for ^{188}Hg, shown in Fig. 5. The fission valley is stabilized to quite large elongations; the calculations show it exists up to $(Q_2/\mathrm{b})^{(1/2)} \approx 13$ where its energy is 9.9 MeV and the mass division $A_{\mathrm{H}}/A_{\mathrm{L}} = 111/77$.

In Ref. [7] and in the summary discussion above, we could give arguments about the expected mean mass asymmetry in fission of ^{180}Hg only because the compound-nucleus energy was sufficiently low that the fission valley, which is protected by the very high ridge, defined the asymmetry of the system until the nascent fragments were almost fully formed. But in other systems, for example ^{174}Hg, such arguments are not possible. The BSM(M) fission-yield model does not suffer from these limitations; it permits us to calculate fission yields for any system at energies above the fission saddle energy. We apply it to the eight even-even Hg isotopes in the range $174 \leq A \leq 188$.

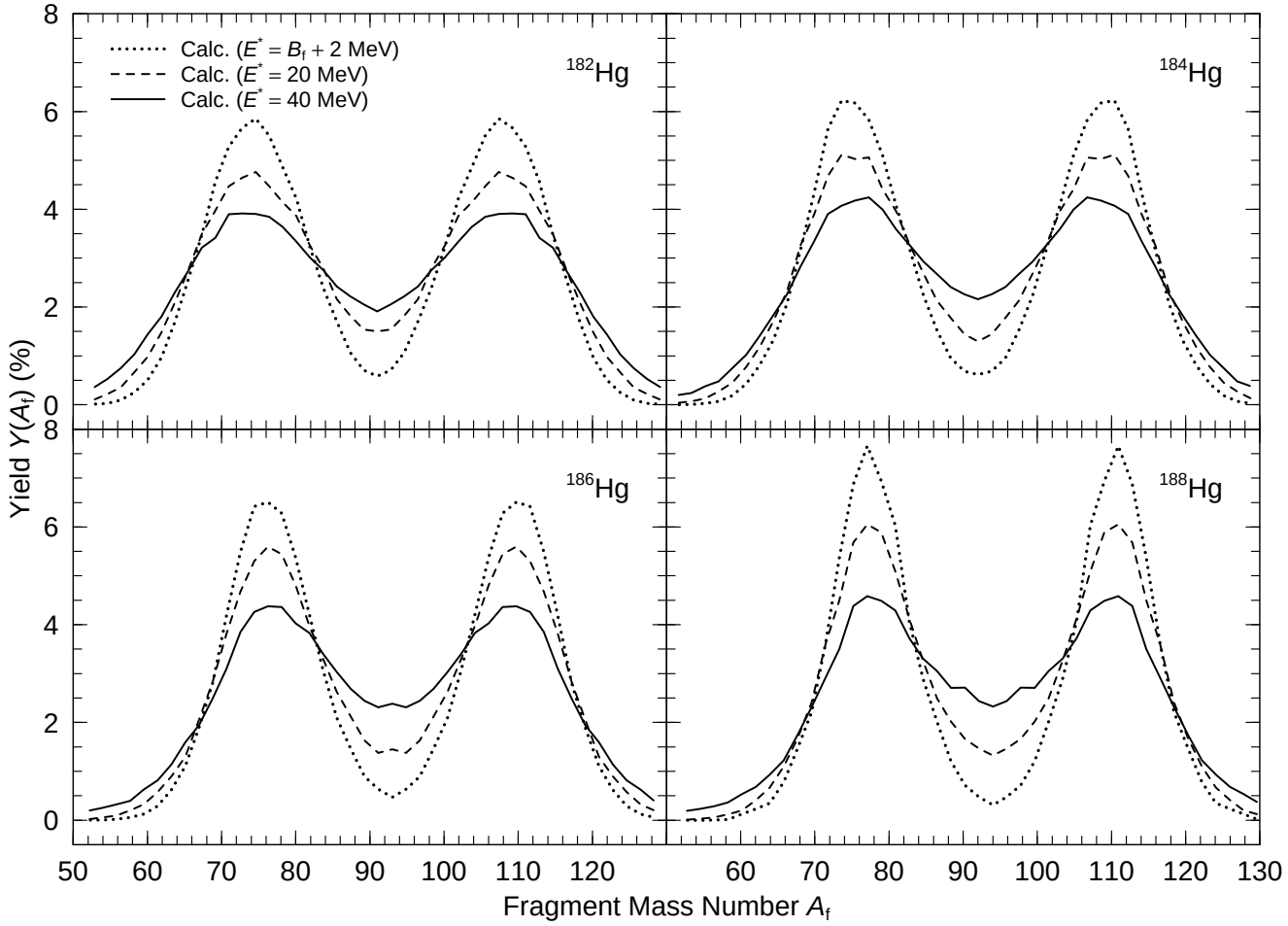

FIG. 7. Calculated yields for four Hg isotopes at three excitation energies. For ^{188}Hg the starting point is the outermost minimum, just inside the saddle and the lowest-energy curve is based on 10000 trajectories rather than 50000 for all other yield curves. The yields become more sharply asymmetric for heavier isotopes.

IV. CALCULATED YIELDS FOR ^{174}Hg–^{188}Hg

In order to calculate the fragment mass yields for the eight neutron-deficient Hg isotopes, we apply the recently introduced method of Brownian shape motion [8]. It involves Metropolis walks on the five-dimensional lattice of 3QS shapes for which the potential energy versus deformation is available [14]. The walks start from the second minimum and terminate when the neck radius drops below a specified value $c_0 = 2.5$ fm. For ^{188}Hg, we start instead in the pronounced third minimum located near $(Q_2/b)^{(1/2)} = 8.5$. As shown in Ref. [16], this procedure is appropriate for shape evolutions in the strongly-damped limit where the inertial masses may be ignored and it provides an exact solution of the associated Smoluchowski transport equation when the dissipation is isotropic. Because the mass yields $P(A_f)$ are rather insensitive to the specific structure of the dissipation tensor, the simple Metropolis procedure represents a good first approximation. More refined calculations would require detailed knowledge of the shape-dependent dissipation tensor, which is not yet well understood.

Figs. 6 and 7 show calculated yields for eight even Hg isotopes from ^{174}Hg to ^{188}Hg. For each isotope we have calculated the yield for three different excitation energies: 2 MeV above the calculated saddle energy, 20 MeV, and 40 MeV.

Experimental data exist only for fission of ^{180}Hg from states below $Q_{EC} \approx 10.5$ MeV, populated in electron capture on ^{180}Tl [7]. The experimental analysis indicates a mass yield that is clearly asymmetric, with the most probable heavy and light masses of $A_H = 100$ and $A_L = 80$, respectively, with a width $\sigma = 4$, and with an uncertainty of the locations of the peaks of ≈ 1 [7]. Our previous theoretical analysis, based purely on static arguments obtained "an asymmetry smaller than $A_H/A_L = 108/72$" [7]. We note that the calculated yields for ^{180}Hg become narrower as the compound-system energy decreases. At the lowest energy, 2 MeV above the barrier, the maximum moves toward the observed asym-

metry of 100/80; in the discrete grid used in the calculations the maximum is at $A_L \approx 75.6$, only 4.4 below the stated experimental value. The BSM(M) model is applicable only to fission at energies above the fission saddle-point energy and cannot at present describe fission below the barrier, at which energies most of the observed experimental yield originates. Therefore the differences between the calculated and the experimental EC-delayed fission yields do not necessarily indicate a problem with the model.

The discovery of asymmetric fission in ^{180}Hg was unexpected from simple systematic extrapolations. Our calculated results for the sequence ^{174}Hg–^{188}Hg show interesting systematic trends in the calculated yields both as a function of neutron number and as a function of energy. Systematic experimental studies would greatly aid efforts to further refine theoretical models.

The following trends in the calculated fission-fragment mass distributions in Figs. 6 and 7 are particularly notable:

- For the lighter isotopes the yield distributions are flatter and less dependent on energy than in the heavier region.

- For ^{174}Hg and ^{176}Hg the yield distribution becomes *more* symmetric with *decreasing* energy, for ^{174}Hg this feature is *very* strong. For the heavier isotopes the distributions become *less* symmetric with *decreasing* energy, that is, the peak-to-valley ratio decreases with increasing energy, the "normal" behavior. Thus it would be highly valuable to test experimentally the theoretical prediction of an anomalous energy dependence for the lighter Hg isotopes.

V. CONCLUDING DISCUSSION

In our previous studies and benchmarking of the BSM(M) model we applied it to nuclei from light Th isotopes to heavy Fm isotopes, that is across most of the actinide region. We obtained encouraging agreement with experimental data across this entire region, including the changing asymmetry with neutron number of the observed yields in Th and the onset of narrow symmetric yields near ^{258}Fm [8, 17]. Some of our results indicated that it is the combined influence of structures in the potential-energy surface in the entire deformation range from the second minimum to near scission that governs the final yields, not just saddle-region properties, scission-region properties, or final "fragment-shell" properties, assumptions that are often the basis of more phenomenological fission-yield models.

But, in the actinide region the effects of the $Z = 50$ and $N = 82$ shells are so strong that they appear very early in the division process, already very near the outer fission saddle point. Therefore, the agreement with experimental data in previous studies is partly related to the description of this very dominant feature in the potential-energy surface. We would remark, however, that while our description of the average heavy-fragment mass in actinide fission arises naturally from the properties of the potential surface before scission [12], consideration of fragment shell effects alone often [4, 5] requires postulating an additional highly deformed shell at $N \approx 88$ along with the spherical shell at $N = 82$ in order to arrive at the observed mass. In the Hg isotopes there is no such obvious dominant feature so the asymmetry observed here is, as previously pointed out [7], a new type of asymmetric fission that has its origins in the more local properties of the potential-energy surface, which are less general, less dominant, and difficult to intuitively anticipate because the potential energy is a complicated surface in the multi-dimensional space of nuclear shapes. By "local" we mean that a specific yield character extends only over a limited range in N and Z and is due to properties of the potential-energy surface over a limited deformation range somewhat beyond the saddle region but not persisting to scission. These properties cannot be anticipated from microscopic effects in the fragments, which are weak here and do not survive to near the saddle.

In contrast, in the actinide region many simple, almost hand-waving arguments have, because of the strong shell effects there, historically "explained" fission yields fairly well. But, in our judgment, the fairly good reproduction of the experimental data in those regions does not convincingly show that the essential physics of the fission process has been correctly identified, because the applicability of the models seems limited to nuclei in the vicinity of the actinide region. The neutron-deficient Hg region offers more challenges than the actinide region but also opportunities to develop fission-yield models with better predictive power. To further study these new drivers of fission properties, detailed comparisons between calculations such as those here and new experimental data can be expected to add to our understanding of the many aspects of fission.

ACKNOWLEDGMENTS

Comments from A. Iwamoto and T. Ichikawa are acknowledged. This work was supported by the Office of Nuclear Physics in the U.S. Department of Energy's Office of Science under contract No. DE-AC02-05CH11231 (J.R.) and JUSTIPEN/UT grant No. DE-FG02-06ER41407 (P.M.), and by the National Nuclear Security Administration of the U.S. Department of Energy at Los Alamos National Laboratory under Contract No. DE-AC52-06NA25396 and the U.S. Department of Energy through the LANL/LDRD Program. (P.M. and A.J.S.)

[1] K.-H. Schmidt, S. Steinhäuser, C. Böckstiegel, A. Grewe, A. Heinz, A. R. Junghans, J. Benlliure, H.-G. Clerc, M. de Jong, J. Müller, M. Pfützner, and B. Voss, Nucl. Phys. **A665** (2000) 221.

[2] M. G. Itkis, N. A. Kondrat'ev, S. I. Mul'gin, V. N. Okolovich, A. Ya. Rusanov, and /G. N. Smirenkin, Yad. Fiz. **52** (1990) 944.

[3] M. G. Itkis, N. A. Kondrat'ev, S. I. Mul'gin, V. N. Okolovich, A. Ya. Rusanov, and G. N. Smirenkin, Yad. Fiz. **53** (1991) 1225.

[4] B. D. Wilkins, E. P. Steinberg, and R. R. Chasman, Phys. Rev. C **14** (1976) 1832.

[5] K.-H. Schmidt, J. Benlliure, and A.R. Junghans, Nucl. Phys. A **693** (2001) 169.

[6] S. I. Mulgin, K.-H. Schmidt, A. Greve, S. v. Zhdanov, Nucl. Phys. A **640** 1998 375.

[7] A. N. Andreyev, J. Elseviers, M. Huyse, P. Van Duppen, S. Antalic, A. Barzakh, N. Bree, T. E. Cocolios, V. F. Comas, J. Diriken, D. Fedorov, V. Fedosseev, S. Franchoo, J. A. Heredia, O. Ivanov, U. Köster, B. A. Marsh, K. Nishio, R. D. Page, N. Patronis, M. Seliverstov, I. Tsekhanovich, P. Van den Bergh, J. Van De Walle, M. Venhart, S. Vermote, M. Veselsky, C. Wagemans, T. Ichikawa, A. Iwamoto, P. Möller, and A. J. Sierk, Phys. Rev. Lett. **105** (2010) 252502.

[8] J. Randrup and P. Möller, Phys. Rev. Lett. **106** (2011) 132503.

[9] N. Bohr and J. A. Wheeler, Phys. Rev. **56** (1939) 426.

[10] S. Frankel and N. Metropolis, Phys. Rev. **72** (1947) 914.

[11] V. M. Strutinsky, Nucl. Phys. **A95** (1967) 420.

[12] P. Möller, D. G. Madland, A. J. Sierk, and A. Iwamoto, Nature **409** (2001) 785.

[13] H. Goutte, J. F. Berger, P. Casoll, and D. Gogny, Phys. Rev. C **71** (2005) 24316.

[14] P. Möller, A. J. Sierk, T. Ichikawa, A. Iwamoto, R. Bengtsson, H. Uhrenholt, and S. Åberg, Phys. Rev. C **79** (2009) 064304.

[15] P. Möller, J. R. Nix, and W. J. Swiatecki, Nucl. Phys. **A469** (1987) 1.

[16] J. Randrup, P. Möller, and A. J. Sierk, Phys. Rev. C **84** (2011) 034613.

[17] P. Möller and J. Randrup, Proc. French-Japanese Symposium on Nuclear Structure Problems - Organized in the framework of FJNSP LIA and EFES, Jan 5–8, 2011 Wakoshi, Saitama Prefectecture, Japan, (World Scientific to appear, Los Alamos Preprint LA-UR-11-11012).

[18] N. B. Gove and M. J. Martin, Nucl. Data Tables **10** (1971) 205.

[19] G. Audi, O. Bersillon, J. Blanchot, and A. H. Wapstra, Nucl. Phys. **A729** (2003) 3.

[20] P. Möller and J. Randrup, Nucl. Phys. **A514** (1990) 1.

[21] J. Krumlinde and P. Möller, Nucl. Phys. **A417** (1984) 419.

[22] P. Möller, J. R. Nix, and K.-L. Kratz, Atomic Data Nucl. Data Tables **66** (1997) 131.

[23] P. Möller, A. J. Sierk, R. Bengtsson, H. Sagawa, and T. Ichikawa, Phys. Rev. Lett. **103** (2009) 212501.

[24] P. Möller and J. R. Nix, Nucl. Phys. **A272** (1976) 502.

[25] P. Möller and J. R. Nix, Nucl. Phys. **A281** (1977) 354.